nature materials

SUPPLEMENTARY INFORMATION

DOI: 10.1038/NMAT3378

Long-range transfer of electron–phonon coupling in oxide superlattices

N. Driza,[1] S. Blanco-Canosa,[1] M. Bakr,[1] S. Soltan,[1,2] M. Khalid,[1] L. Mustafa,[1] K. Kawashima,[1] G. Christiani,[1] H.-U. Habermeier,[1] G. Khaliullin,[1] C. Ulrich,[1,3,4] M. Le Tacon,[1] and B. Keimer[1]

[1]*Max-Planck-Institut für Festkörperforschung, Heisenbergstr. 1, D-70569 Stuttgart, Germany*

[2]*Faculty of Science, Helwan University, 11795-Cairo, Egypt*

[3]*University of New South Wales, School of Physics, 2052 Sydney, New South Wales, Australia*

[4]*The Bragg Institute, Australian Nuclear Science and Technology Organization, Lucas Heights, NSW 2234, Australia*

DOI: 10.1038/NMAT3378

A. Sample preparation and characterization

YBCO/LCMO superlattices were grown by pulsed laser deposition on 5×5 mm^2 $SrTiO_3$ (STO) substrates with (001) orientation.[1] During the deposition process, the substrate was kept at a constant temperature of 730°C, and the oxygen partial pressure in the deposition chamber was 0.5 mbar. Afterwards the films were annealed *in situ* at 530°C in oxygen at 1.0 bar for 60 min. The high quality of all samples was confirmed by x-ray diffraction, which showed epitaxial growth with the c-axis along (001). This is further demonstrated by the relative intensity of the Raman-allowed phonon modes of YBCO. The onset superconducting and the ferromagnetic transition temperatures (T_c and T_{Curie}, respectively) were measured using a vibrating-sample magnetometer as illustrated in Supplementary Fig. 1. The corresponding transition temperatures (listed in Supplementary Table I) are consistent with previous work.[1,2,3]

B. Reciprocal Space Mapping

In order to quantify the strain state of our samples, we have taken a systematic series of reciprocal space maps (RSMs) on a six-circle x-ray diffractometer using a rotating Cu anode source running at a cathode voltage of 45 kV and a filament current of 120 mA. All RSMs swept the (002) and (013) Bragg reflections of the STO substrate, which were also used to align the sample and define the orientation matrix. The scattered radiation was detected using a Mythen detector which consists of a linear array of reversed-biased silicon diodes. No background subtraction was made in the Region Of Interest (ROI) defined for the Mythen detector.

In Supplementary Fig. 2a, we show the RSM of a 40 nm thick thin reference film of $La_{2/3}Ca_{1/3}MnO_3$. The intense peak around $Q_x = 1.61$ Å^{-1} and $Q_z = 4.83$ Å^{-1} corresponds to the (013) Bragg reflection of the STO substrate, while the peak at $Q_x = 1.61$ Å^{-1} and $Q_z = 4.96$ Å^{-1} originates from the LCMO layer. In this case, the in-plane lattice parameters of LCMO match perfectly the ones of STO, and the film is fully strained. This film has not been characterized by Raman scattering due to its low thickness. Supplementary Fig. 2b shows the same RSM for our 300 nm thick film of $La_{2/3}Ca_{1/3}MnO_3$. The diagonal line has a slope $l/k = 1$, and corresponds to the expected position of the LCMO Bragg peak if the film were fully relaxed. The shift of the Bragg peak away from this line indicates partial relaxation of the substrate-induced strain, which varies as a function of distance from the substrate and hence broadens the peak profile,

as expected for films of this thickness. The mean lattice parameters of the film measured from the off-specular diffraction data at room temperature are $a = b = 3.862$ Å and $c = 3.832$ Å, while bulk LCMO of this composition has a (pseudocubic) lattice parameter of 3.840 Å. The comparison of the Raman spectrum of this film (Supplementary Fig. 8 below, and Fig. 2a in the main text) with those of bulk $La_{2/3}Ca_{1/3}MnO_3$ demonstrates that the influence of the nonuniform strain in the film on the phonon profiles is negligible.

Supplementary Fig. 3 shows room-temperature RSMs of two representative SLs with thin (15 nm) and thick (50 nm) YBCO layers. In the RSMs of the (Y-15 nm/L-10 nm)$_{15}$ SL, the first and second SL satellites are well resolved around the LCMO (002) and (013) reflections. The (006) reflection of YBCO overlaps the (002) reflection of the STO substrate (Fig. 3a, left panel), but the (109)/(019) reflection of YBCO can be clearly separated from the (013) reflection of STO (right panel). For the (Y-50 nm/L-10 nm)$_5$ SL, the superlattice satellites are much more closely spaced because of the larger SL periodicity, and hence no longer well resolved in the RSMs (Fig. 3b). Nonetheless, both in-plane and out-of-plane lattice parameters can be determined with reasonable accuracy from the (013) RSMs. We also note that the LCMO (013) reflection is even closer to the line indicating full relaxation than the one in the LCMO film above. Combined with the x-ray and Raman data on the reference films, these data allow us to safely rule out any major influence of substrate-induced strain on the Raman scattering measurements on the superlattices.

From a temperature series of analogous RSMs (Supplementary Figs. 4 and 5), we have extracted the lattice parameters of both superlattices (Supplementary Fig. 6), which are nearly identical to those in the bulk. In particular, there is no indication of any anomaly in the thermal expansion that could be tied to the phonon anomalies we observed. Likewise, we did not observe any significant temperature dependent intensity shift in the RSMs that could be indicative of an anomalous internal rearrangement of the ions in the unit cell. The negligible influence of mutual strain implied by these data is not unexpected, because the in-plane lattice parameters of YBCO and LCMO differ by less than 0.3%.

In summary, the RSMs demonstrate explicitly that neither substrate-induced nor mutual strain can be responsible for the phonon anomalies reported in the main text, supporting our conclusion that they arise from the dynamical electron-phonon interaction.

DOI: 10.1038/NMAT3378

C. Raman Experiments

The Raman scattering experiments were performed in a backscattering geometry using a Horiba-Jobin-Yvon T64000 micro-Raman spectrometer equipped a nitrogen-cooled CCD camera as detector. The 514.5 nm and 488.0 nm Ar^+ laser lines were used for the measurements, and the reported results were found to be independent of the chosen wavelength (Supplementary Fig. 7). The incident laser beam was focussed to a 10 μm spot using a $\times$50, long working distance objective on the sample which was placed on the cold finger of a He-cooled cryostat. The laser power was kept below 1.5 mW to avoid laser-induced heating. The polarization of the electric field of the incident and scattered light was kept parallel to the crystallographic $a-$axis of the YBCO layer.

In the following, we present and discuss reference measurements on two epitaxial LCMO films with different doping levels, and on a bare STO substrate.

1. $La_{2/3}Ca_{1/3}MnO_3$

Supplementary Fig. 8 shows a room-temperature Raman spectrum of the 300 nm thick $La_{2/3}Ca_{1/3}MnO_3$ film whose lattice structure was already discussed above (Supplementary Fig. 2b). The composition of this film is identical to those of the LCMO layers in the superlattices. The spectrum of the epitaxial looks nearly identical (apart from the different background conditions) to the one of a bulk crystal with the same composition previously investigated by Irwin *et al.*[4] In particular, the frequencies of the 230 cm^{-1} phonon in the LCMO film and in the bulk crystal are identical within the measurement error. Fig. 2a in the main text further demonstrates that the 230 cm^{-1} phonon evolves with temperature in a manner precisely identical to the one in bulk samples, including the hardening upon cooling below the Curie temperature induced by the spin-phonon coupling. The influence of the spatially nonuniform strain in the film on the shape of the phonon profiles and their temperature dependence is thus at most very minor.

In agreement with previous Raman work,[4] we observe a strong renormalization of the $A_g(2)$ phonon, which is associated with a staggered rotation of the MnO_6 octahedra, at the ferromagnetic transition temperature T_{Curie} (Fig. 2a in the main text). The phonon hardening is much larger than the one expected from the difference between the static lattice parameters of

the high- and low-temperature phases. Specifically, prior Raman measurements on manganite perovskites at room temperature have demonstrated that the energy of this phonon scales with the tilting angle ψ of the MnO_6 octahedra around the [010] axis of the elementary perovskite unit cell [5]: $\hbar\omega_{A_g(2)} \sim 23.5 \times \psi$ cm^{-1}. The magnetostriction at T_{Curie} in the bulk system cannot explain the strong phonon renormalization, because the MnO_6 octahedra tilting angle only increases by $\sim 0.1°$.[6] According to the formula above, this would cause a hardening of ~ 2 cm^{-1}, while the mode actually hardens by ~ 8 cm^{-1} between 300 and 10 K.

Instead, prior work has demonstrated that the phonon anomaly is a direct consequence of the modification of the electron screening at the Curie temperature, through renormalization of the "double-exchange" bandwidth $t < cos(\frac{\theta_{ij}}{2}) >$ across T_{Curie}, where t is the hopping parameter, θ_{ij} the angle between two adjacent Mn ionic spins, and $< ... >$ stands for thermodynamic average. By virtue of the electron-phonon coupling, the phonon frequency renormalizes as $\sqrt{1 - \beta / < cos(\frac{\theta_{ij}}{2}) >}$, where β is essentially T-independent.[7] Following Ref. 4, we have fitted the temperature dependence of the LCMO $A_g(2)$ phonon frequency using the $< cos(\frac{\theta_{ij}}{2}) >$ value obtained in the mean-field approximation by Kubo and Ohata.[8] The best fit was found for $\beta = 0.17$ (see Fig. 2a of the main text), in excellent agreement with Irwin's results.

2. $La_{1/3}Ca_{2/3}MnO_3$

In order to check the influence of the charge carrier concentration on the behavior of the LCMO $A_g(2)$ phonon, we have also investigated a 300 nm thick film with composition $La_{1/3}Ca_{2/3}MnO_3$ grown by pulsed laser deposition on a $SrTiO_3$ substrate with (001) orientation. At this doping level, the low-temperature ground state is a charge-ordered antiferromagnetic insulator. The Néel temperature of our film determined by magnetometry was $T_N = 150$ K. The temperature dependence of the $A_g(2)$ mode measured with Raman scattering revealed a continuous hardening of the mode frequency upon cooling from room temperature to T_N, followed by a saturation (Supplementary Fig. 9). The softening of the mode observed in our superlattices can therefore not originate from charge transfer effects.

DOI: 10.1038/NMAT3378

3. $SrTiO_3$ substrate

In Raman scattering experiments on epitaxial films, one needs to ensure that the detected signal originates from the film, not from the substrate. Substrate phonons are commonly observed for films of thickness below the penetration depth of the laser light. For reference, we have therefore measured Raman spectra of a bare STO substrate. Supplementary Fig. 10 shows that the STO spectrum is remarkably similar to the one reported by Xiong *et al.*[9] for a $La_{0.67}Ca_{0.33}MnO_3$ film grown on STO. This indicates that the data of Xiong *et al.* reflect the response of the substrate, not the one of the LCMO film. Temperature dependent data on our STO substrate (Supplementary Fig. 11) suggest that the well-known softening of the pertinent STO phonons upon cooling is responsible for the softening of the phonon features reported by Xiong *et al.* Our Raman data were taken on thicker films and are hence not contaminated by substrate phonons.

[1] Soltan, S., Albrecht, J. & Habermeier, H.-U. Ferromagnetic/superconducting bilayer structure: A model system for spin diffusion length estimation. *Phys. Rev. B* **70**, 144517 (2004).

[2] Peña, V. *et al.* Coupling of superconductors through a half-metallic ferromagnet: Evidence for a long-range proximity effect. *Phys. Rev. B* **69**, 224502 (2004).

[3] Holden, T. *et al.* Proximity induced metal-insulator transition in $YBa_2Cu_3O_7/La_{2/3}Ca_{1/3}MnO_3$ superlattices. *Phys. Rev. B* **69**, 064505 (2004).

[4] Irwin, J. C., Chrzanowski, J. & Franck, J. P. Oxygen isotope effect on the vibrational modes of $La_{1-x}Ca_xMnO_3$. *Phys. Rev. B* **59**, 9362-9371 (1999).

[5] Iliev, M. N. *et al.* Distortion-dependent Raman spectra and mode mixing in $RMnO_3$ perovskites (R = La, Pr, Nd, Sm, Eu, Gd, Tb, Dy, Ho, Y). *Phys. Rev. B* **73**, 064302 (2006).

[6] Dai, P. *et al.* Experimental evidence for the dynamic Jahn-Teller effect in $La_{0.65}Ca_{0.35}MnO_3$. *Phys. Rev. B* **54**, R3694-R3697 (1996).

[7] Lee, J. D. & Min, B. I. Polaron transport and lattice dynamics in colossal-magnetoresistance manganites. *Phys. Rev. B* **55**, 2454-12459 (1997).

[8] Kubo, K. & Ohata, N. A. Quantum Theory of Double Exchange. I. *J. Phys. Soc. Jpn.* **33**, 21-32 (1972).

[9] Xiong, Y. M. *et al.* Raman spectra in epitaxial thin films of $La_{1-x}Ca_xMnO_3$ (x = 0.33, 0.5) grown on

different substrates. *Phys. Rev. B* **70**, 094407 (2004).

DOI: 10.1038/NMAT3378

Sample	YBCO Thickness	LCMO Thickness	T_c	T_{Curie}
bulk LCMO	0 nm	300 nm	-	275 K
(Y-5 nm/L-10 nm)$_{20}$	5 nm	10 nm	35 K	235 K
(Y-10 nm/L-10 nm)$_{15}$	10 nm	10 nm	45 K	230 K
(Y-20 nm/L-10 nm)$_{10}$	20 nm	10 nm	60 K	220 K
(Y-30 nm/L-10 nm)$_{7}$	30 nm	10 nm	82 K	185 K
(Y-50 nm/L-10 nm)$_{5}$	50 nm	10 nm	82 K	230 K
bulk YBCO	300 nm	0 nm	90K	-

Table I: Properties of the samples studied in this work. The columns denote the YBCO and LCMO thicknesses and the superconducting and ferromagnetic transition temperatures, respectively. The total thickness of the samples was kept between 250 and 300 nm in order to avoid any influence of the substrate on the Raman signal.

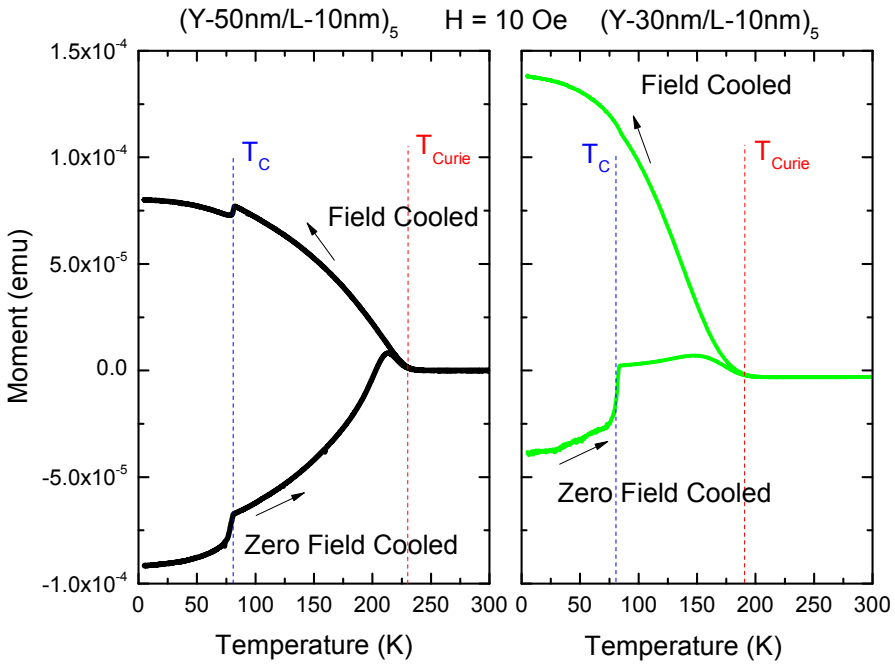

Fig. 1: **Supplementary Material.** Typical magnetization measurements, shown here for the (Y-50 nm/L-10 nm)$_5$ (left panel) and (Y-30 nm/L-10 nm)$_7$ (right panel) superlattices.

DOI: 10.1038/NMAT3378

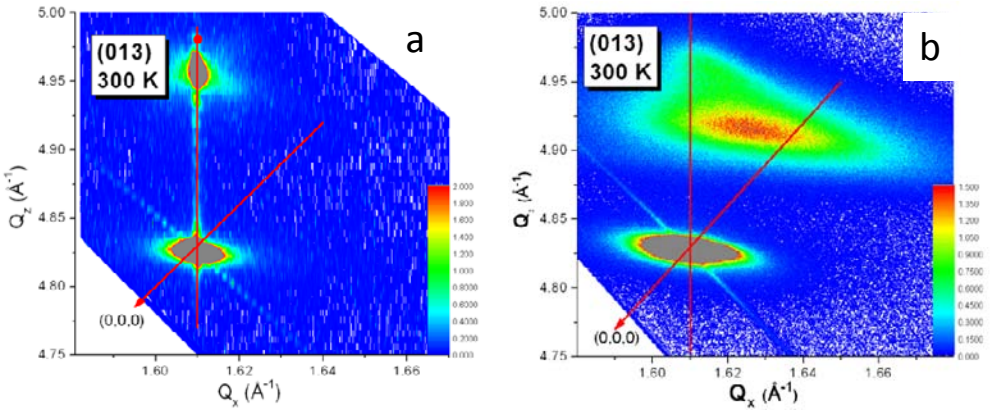

Fig. 2: **Supplementary Material.** RSMs of (a) 40 nm and (b) 300 nm thick $La_{2/3}Ca_{1/3}MnO_3$ films.

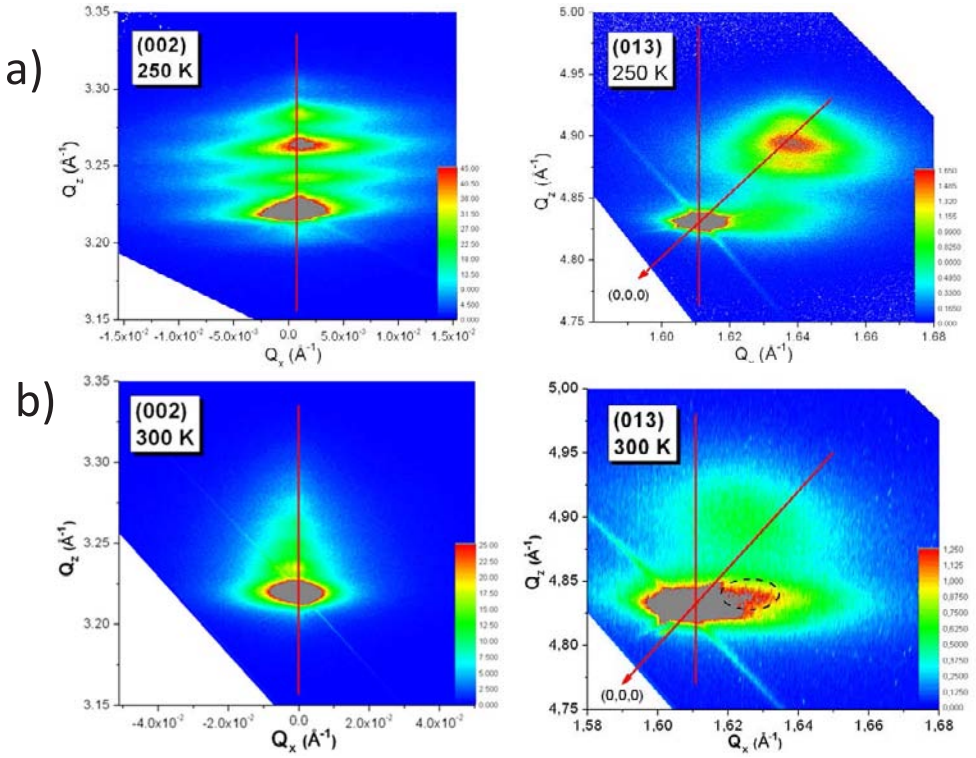

Fig. 3: **Supplementary Material.** RSMs of (a) (Y-15 nm/L-10 nm)$_{15}$ and (b) (Y-50 nm/L-10 nm)$_5$ superlattices. The dashed line in panel (b) indicates the (109)/(019) Bragg reflection of YBCO, which partially overlaps the (103) reflection of the STO substrate.

DOI: 10.1038/NMAT3378

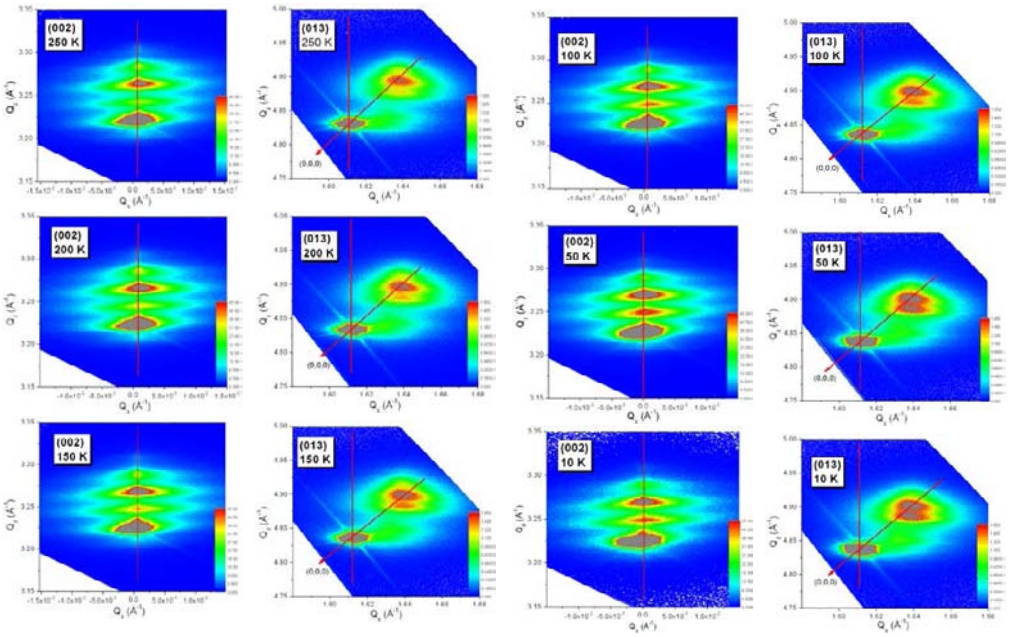

Fig. 4: **Supplementary Material.** RSMs of a (Y-15 nm/L-10 nm)$_{15}$ superlattice at various temperatures.

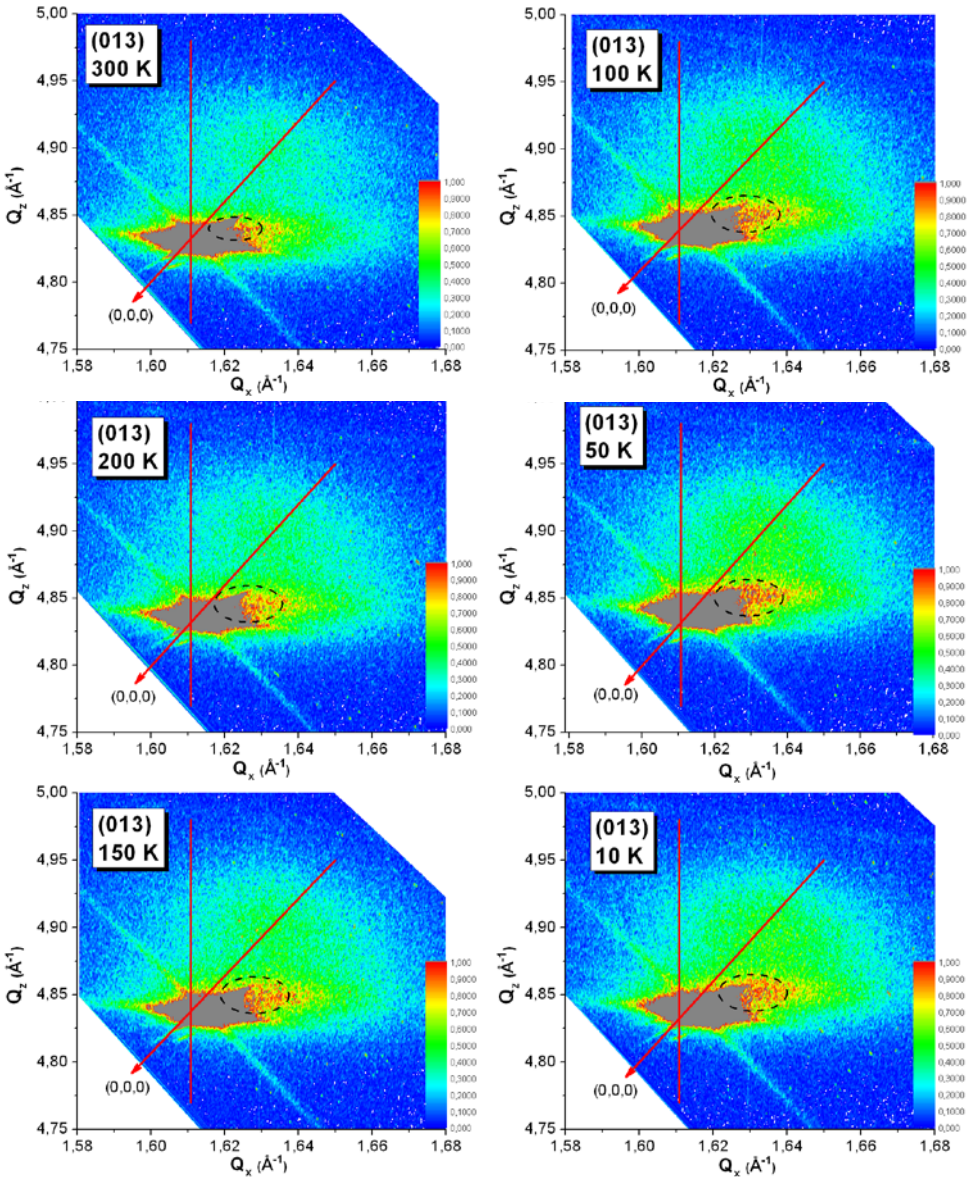

Fig. 5: **Supplementary Material.** RSMs of a (Y-50 nm/L-10 nm)$_5$ superlattice at various temperatures.

DOI: 10.1038/NMAT3378

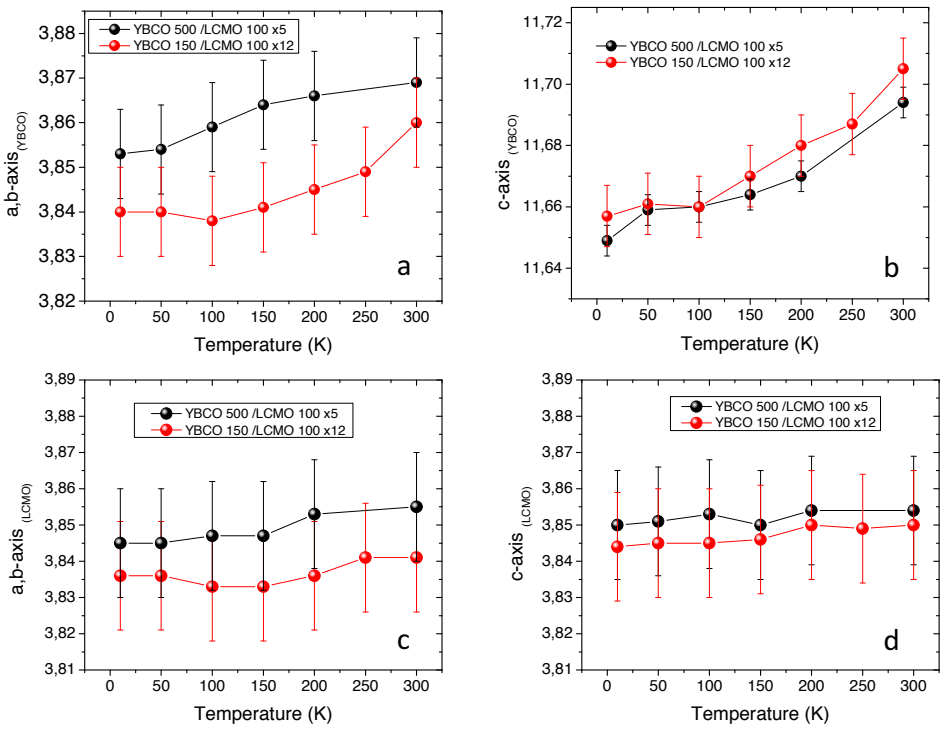

Fig. 6: **Supplementary Material.** Temperature dependent lattice parameters of the (a,b) YBCO layers and (c,d) LCMO layers in two representative superlattices.

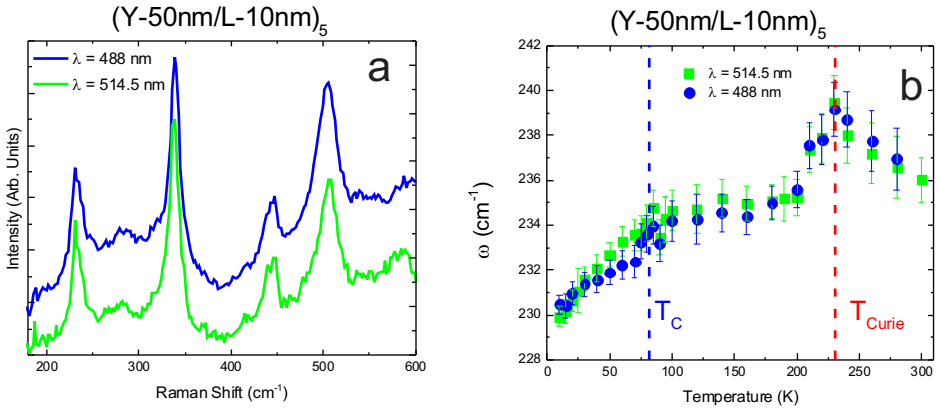

Fig. 7: **Supplementary Material.** a) Raman spectra of (Y-50 nm/L-10 nm)$_5$ superlattice at T= 15 K measured with blue (λ = 488 nm) and green (λ = 514.5 nm) laser light. For clarity the spectra were normalized and vertically shifted by a constant offset. b) Temperature dependence of the $A_g(2)$ phonon frequency measured for these two wavelengths. The error bars reflect the accuracy of the fitting procedure.

DOI: 10.1038/NMAT3378

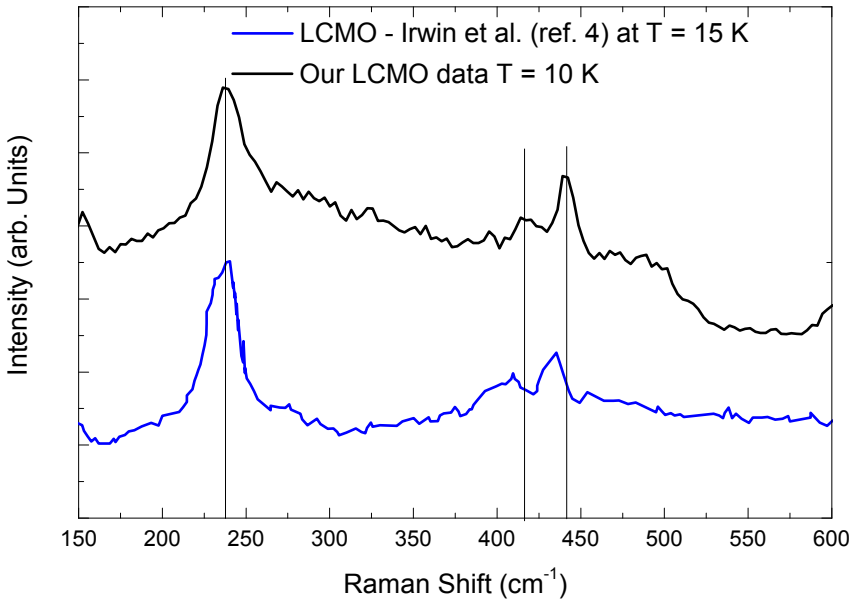

Fig. 8: **Supplementary Material.** Comparison of the Raman spectra measured on our 300 nm thick $La_{2/3}Ca_{1/3}MnO_3$ film and the data from Irwin *et al.*[4] on bulk LCMO.

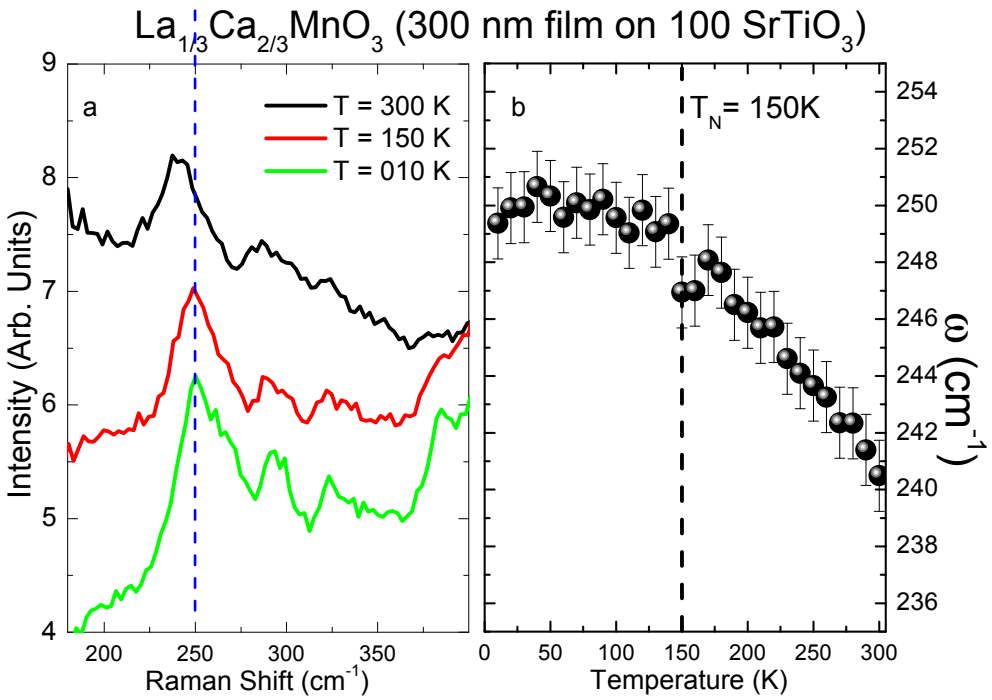

Fig. 9: **Supplementary Material.** a) Raman spectra of an overdoped $La_{1/3}Ca_{2/3}MnO_3$ film at T= 300, 150, and 10 K. For clarity each spectrum is vertically shifted by a constant offset. b) Temperature dependence of the $A_g(2)$ phonon frequency.

DOI: 10.1038/NMAT3378

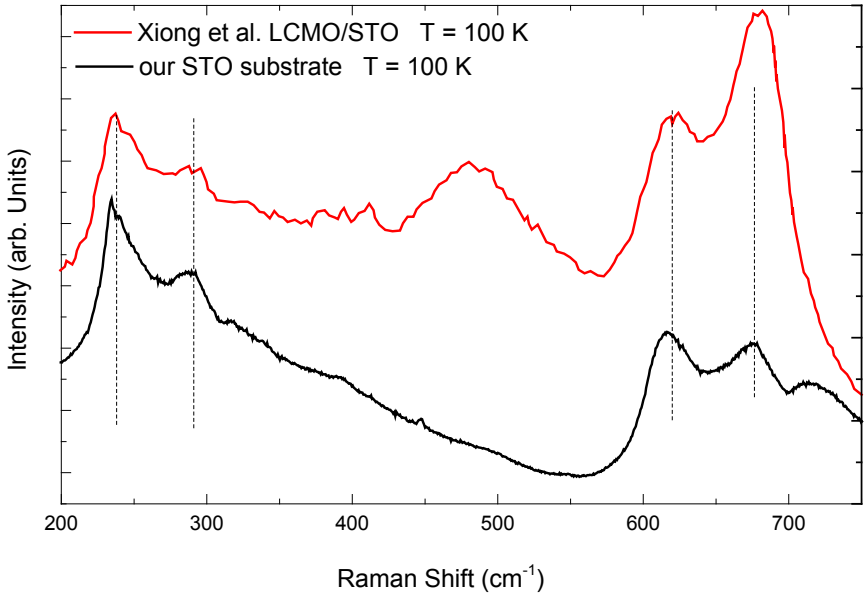

Fig. 10: **Supplementary Material.** Raman spectrum of a bare STO substrate at room temperature, in comparison to the spectrum of an LCMO film grown on STO reported by Xiong *et al.*[9]

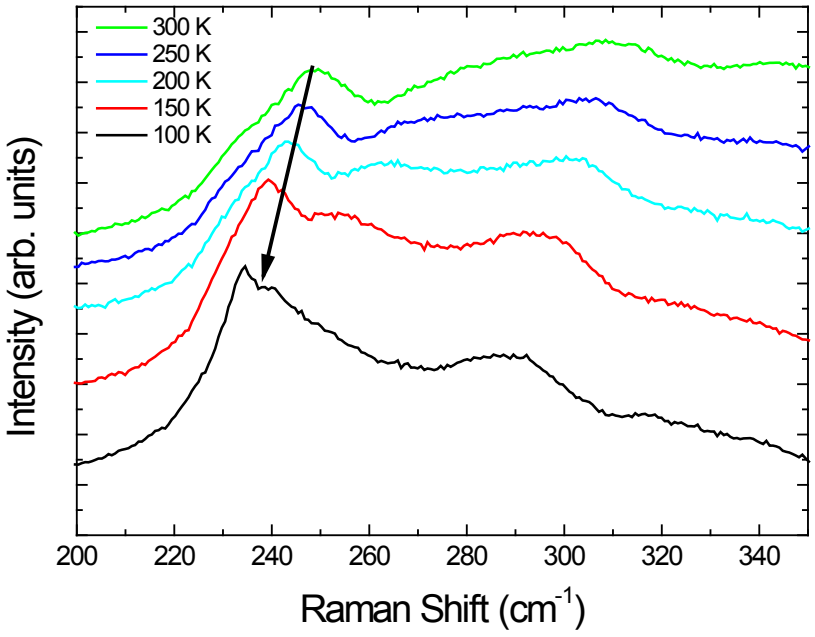

Fig. 11: **Supplementary Material.** Raman spectra of a bare STO substrate at various temperatures. For clarity the spectra were normalized and vertically shifted by a constant offset.